Title

Effect of shift in refractive index of dispersive elements in waveband-shift-free optical phase conjugator based on DFG

The names of authors

YASUHIRO OKAMURA[1,*] AND ATSUSHI TAKADA[1]

The affiliation of the authors

Faculty of Science and Engineering, Tokushima University, 2-1 Minamijosanjima, Tokushima-shi, Tokushima 770-8506, Japan

E-mail address of the corresponding author

*okamura.yasuhiro@tokushima-u.ac.jp

Abstract

In this study, the effect of the shift in the refractive index between two dispersive elements on the output phase-conjugated (PC) wave power of waveband-shift-free optical-phase conjugators based on difference-frequency generation (DFG-OPCs) is analyzed. First, a numerical model of the DFG-OPC is built by considering the shift Δn in the refractive index. The derived formula shows that the output PC wave power of DFG-OPCs depends on the shift in the refractive index. Subsequently, the dependence of the output PC wave power on the shift is confirmed analytically. Calculations indicate that the output PC wave power varies according to the shift. For a relatively fractional shift Δn = 1.0e-6, the output PC power is degraded by 3 dB. Finally, acceptable values of the shift and temperature difference are calculated as functions of the length of the dispersive element. It is illustrated in this study that the acceptable value of shift in the refractive index increases as the length of the dispersive element is reduced and that the output PC wave power can be stabilized against changes in temperature.

Keywords

Optical Nonlinear Compensation, Optical Phase Conjugation, Waveband-Shift-Free, Difference-Frequency Generation, Refractive Index Shift, Dispersive Elements

Declarations

Funding (information that explains whether and by whom the research was supported)
Not applicable

Conflicts of interest/Competing interests (include appropriate disclosures)
Not applicable

Availability of data and material (data transparency)
The data that support the findings of this study are available from the corresponding author upon reasonable request.

Code availability (software application or custom code)
The data that support the findings of this study are available from the corresponding author upon reasonable request.

1. Introduction

To accommodate the increase in Internet traffic, higher speed and spectrally efficient optical fiber communication systems are required [1]. One factor that limits high-speed optical fiber transmission is the optical nonlinear degradation caused by the nonlinearity of the fiber [2, 3]. Optical nonlinear compensation using digital signal processing (DSP) algorithms, e.g., digital backpropagation [4, 5], Volterra series transfer function [6], and artificial neural networks [7, 8], are successful technologies that can mitigate degradations in signals caused by optical nonlinearity. For further improvement in the quality of the received signal, the combination of a DSP technique and an optical signal processing (OSP) technique is beneficial. Non-degenerate phase-sensitive optical amplifiers (PSAs) have recently received broad attention because not only low-noise amplification but also nonlinear phase noise compensation can be achieved in the optical domain [9-13]. However, the PSAs require phase-conjugated twin wave transmission [14] which halves spectral efficiency (SE). In the meantime, optical phase conjugator (OPC) [15-26] is based on an OSP technique and has the potential to reduce the computational cost of receiver-side DSP calculations. This is because the signal degradations caused by chromatic dispersion and optical nonlinearity are simultaneously compensated by the OPC in the optical domain and contribute to reducing the computational load on receiver-side DSP. An OPC is placed in the middle of the transmission fibers, where it generates a phase-conjugate (PC) wave of a signal wave transmitted through the first half of the span. The generated PC wave includes inverted distortion arising from linear and nonlinear impairments in the first half of the span and is launched into the second half of the span. After transmission, the distortions of the first and second halves of the spans are canceled. However, in conventional OPCs, the wavelengths of the PC waves are shifted from those of the signal waves during generation [15]. Therefore, a waveband must be reserved for the PC waves, and this leads to the degradation of SE. Recently, waveband-shift-free OPCs, which generate spectrally inverted PC waves of the incoming wavelength-division multiplexed (WDM) signal waves at the same center wavelength as that of the WDM signal waves, have been demonstrated to mitigate the degradation of the SE [16-22]. Such OPCs are classified into two types—one based on four-wave mixing (FWM) and the other based on difference-frequency generation (DFG). The FWM-based OPCs [16-20] employs dual pumps for PC wave generation and requires guard bands to avoid nonlinear crosstalk among the incoming WDM signal waves via the pumps. This leads to the degradation of the SE. Furthermore, it is difficult to generate PC waves from broad WDM signal waves owing to phase matching in an optical $\chi^{(3)}$ nonlinear medium for FWM. The DFG-based OPCs enable broadband PC wave generation because of the optical $\chi^{(2)}$ nonlinear medium for DFG [21, 22]. In the experimental demonstration [21], only a 25-GHz guard band is required at the center channel of the WDM signal waves. However, there is still scope to improve the SE and its configuration, including wavelength-selective switches. On the other hand, we propose and numerically investigate waveband-shift-free OPC based on DFG

(DFG-OPC) [23], which is inspired by the studies [24, 25]. The DFG-OPC does not require the guard band of the center channel of the WDM signal waves and is composed of a Sagnac loop interferometer (SLI), including an optical nonlinear medium and dispersive elements (DEs). The signal and pump wave are launched into the SLI, and a PC wave with the same center wavelength as the signal wave is generated by an optical $\chi^{(2)}$ nonlinear medium such as a periodically poled lithium niobate (PPLN) waveguide. Subsequently, PC waves generated from the input waves with clockwise and counterclockwise rotation interfere with a specific phase difference caused by the DEs, and only the PC wave is output from the output port.

In our previous study [23], it was assumed that the phase constants between two DEs were identified. However, in reality, the refractive indexes of the DEs change owing to fluctuations in temperature, which affect the output PC wave power. In the conference paper [26], as an initial verification step, we have analytically studied the effect of the shift in the refractive indexes of the DEs in a DFG-OPC circuit, and the degradation in the output PC wave power owing to the shift in the refractive index has been confirmed. However, quantitative evaluations have been insufficient, and the relationship between the degradation in the output PC wave power and the shift in the refractive indexes of the DEs has not been clarified in detail.

This study is an extension of [26]. First, we mathematically show the effect of the shift in the refractive indexes between the DEs on the DFG-OPC circuit and calculate the output PC wave power as a function of the difference in the lengths of the DEs under circumstances in which the shift is not equal to zero. Thereafter, it is numerically investigated that degradation of the output PC power depends on the shift in the refractive indexes. Finally, an acceptable value of the shift in the refractive indexes of the DEs is determined to obtain stable output PC wave power from DFG-OPCs. In this paper, standard single-mode fibers (SSMFs) are assumed to be used as DEs even though there are many types of DEs such as silicon, polymer, silica, and lithium niobate waveguides. This is because the SSMFs are well compatible with the fiber-pigtailed components which would be used for the future experimental demonstration of DFG-OPC.

2. Mathematical expression of effect of refractive index on DFG-OPCs

In the DFG-OPC, a PC wave with the maximum power can be obtained when the phase difference between the clockwise and counterclockwise propagating PC waves generated in an SLI is appropriately adjusted using DEs. However, the phase shift for the PC waves is determined by not only the lengths of the DEs but also the phase constants of the DEs, depending on the refractive indexes of the DEs and the wavelengths of the PC waves. Therefore, there is a concern that the output PC wave power will decrease owing to the shift in the refractive indexes between the DEs. In this section, we formulate the effect of this shift on the output PC wave power.

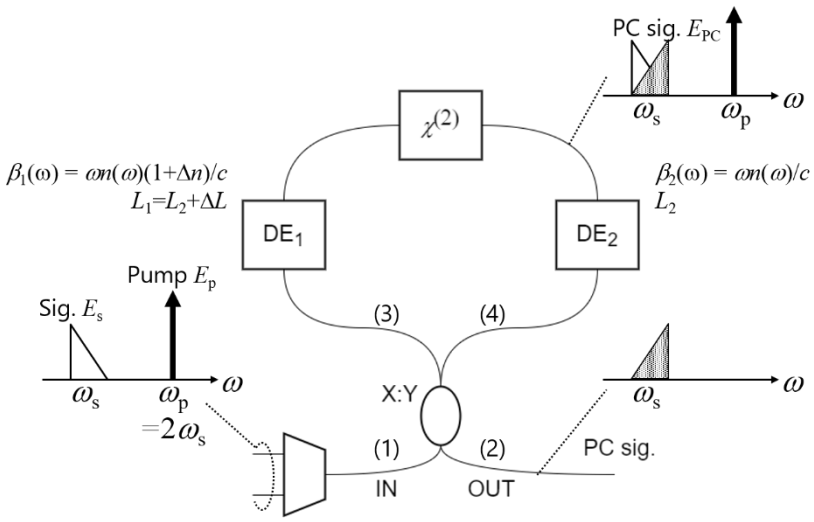

Fig. 1 DFG-OPC model

Figure 1 presents the schematic of a DFG-OPC enabling waveband-shift-free PC wave generation. As depicted in Fig. 1, the DFG-OPC is composed of an SLI consisting of an optical 3-dB coupler (CPL), two DEs, and a $\chi^{(2)}$ optical nonlinear material. First, a signal and pump waves with complex electric field amplitudes E_s and E_p are input to port 1 of the CPL. Here, the central optical angular frequencies of the signal and pump waves are ω_s and ω_p ($=2\omega_s$), respectively. These waves are divided into two parts and output from ports 3 and 4, respectively, of the CPL. For the clockwise propagation of the SLI, the signal and pump waves are phase-shifted by DE_1 with a phase constant $\beta_1(\omega)$ ($= n_1(\omega)\omega/c$) and length L_1. Thereafter, the phase-shifted signal and pump waves are guided into $\chi^{(2)}$ optical nonlinear material such as a PPLN waveguide, and PC waves, E_{PC}, with an optical angular frequency $\omega_{PC} = \omega_p - \omega_s$ are generated through the DFG process. The DFG process can be expressed as the following analytical solution of mode-coupled equations under the assumption that pump depletion and $\chi^{(2)}$ waveguide loss are negligible [27]:

$$\begin{cases} E_{\mathrm{s}}(z)e^{j\Delta kz/2} = E_{\mathrm{s}}(0)\left[\cosh(sz)+\dfrac{j\Delta k}{2s}\sinh(sz)\right]-j\dfrac{g}{2s}E_{\mathrm{PC}}^{*}(0)\sinh(sz) \\ E_{\mathrm{PC}}^{*}(z)e^{-j\Delta kz/2} = E_{\mathrm{PC}}^{*}(0)\left[\cosh(sz)-\dfrac{j\Delta k}{2s}\sinh(sz)\right]+j\dfrac{g^{*}}{2s}E_{\mathrm{s}}(0)\sinh(sz) \end{cases} \quad (1)$$

In Eq. (1), the phase mismatching coefficient Δk can be expressed as $\Delta k = |k_{\mathrm{p}} - k_{\mathrm{s}} - k_{\mathrm{PC}}| - 2\pi/\Lambda$, where k_{p}, k_{s}, and k_{PC} and Λ are the phase constants of the pump, signal, and PC waves and the polarization-inverted period for quasi-phase matching, respectively. The gain coefficient $g = \kappa E_p(0)$, where κ is the coupling coefficient. Further, $s = \sqrt{|g/2|^2 - (\Delta k/2)^2}$. Therefore, the PC, signal, and pump waves are phase-shifted by DE_2 with a phase constant $\beta_2(\omega)$ and length L_2 and input to port 4 of the CPL. Similarly, the PC, signal, and pump waves propagating counterclockwise of the SLI are input to port 3 of the CPL and made to interfere with the clockwise propagating waves. The output PC wave power from ports 1 and 2 of the CPL can be described as follows:

$$\begin{aligned} P_{\mathrm{PC1}} &\propto \left|\frac{E_{\mathrm{CCW}}^{\mathrm{PC}}}{\sqrt{2}}-\frac{jE_{\mathrm{CW}}^{\mathrm{PC}}}{\sqrt{2}}\right|^2 \\ &= P_{\mathrm{PC}}+P_{\mathrm{PC}}\sin\left[\left\{\beta_2(\omega_{\mathrm{p}})-2\beta_2(\omega_{\mathrm{s}})\right\}L_2-\left\{\beta_1(\omega_{\mathrm{p}})-2\beta_1(\omega_{\mathrm{s}})\right\}L_1\right] \end{aligned} . \quad (2)$$

$$\begin{aligned} P_{\mathrm{PC2}} &\propto \left|\frac{E_{\mathrm{CW}}^{\mathrm{PC}}}{\sqrt{2}}-\frac{jE_{\mathrm{CCW}}^{\mathrm{PC}}}{\sqrt{2}}\right|^2 \\ &= P_{\mathrm{PC}}-P_{\mathrm{PC}}\sin\left[\left\{\beta_2(\omega_{\mathrm{p}})-2\beta_2(\omega_{\mathrm{s}})\right\}L_2-\left\{\beta_1(\omega_{\mathrm{p}})-2\beta_1(\omega_{\mathrm{s}})\right\}L_1\right] \end{aligned} . \quad (3)$$

Here, $E_{\mathrm{CW}}^{\mathrm{PC}}$ and $E_{\mathrm{CCW}}^{\mathrm{PC}}$ denote the complex electric field amplitude of the PC waves with clockwise and counterclockwise propagation, and $P_{\mathrm{PC}} = \kappa^2|E_{\mathrm{s}}E_{\mathrm{p}}|^2\sinh^2(sz)/16s^2$. Subsequently, we introduce the shift in the refractive index, Δn (= $n_1/n_2 - 1$), between the two DEs and the difference in DE lengths, ΔL (= $L_1 - L_2$), and substitute them to Eqs. (2) and (3). Therefore,

$$P_{\mathrm{PC1}} \propto P_{\mathrm{PC}}+P_{\mathrm{PC}}\sin\left[\left\{2\beta_2(\omega_{\mathrm{s}})-\beta_2(\omega_{\mathrm{p}})\right\}\left\{\Delta L+\Delta n(L_2+\Delta L)\right\}\right] \quad (4)$$

$$P_{\mathrm{PC2}} \propto P_{\mathrm{PC}}-P_{\mathrm{PC}}\sin\left[\left\{2\beta_2(\omega_{\mathrm{s}})-\beta_2(\omega_{\mathrm{p}})\right\}\left\{\Delta L+\Delta n(L_2+\Delta L)\right\}\right] \quad (5)$$

Here, P_{PC2} is the PC wave power from port 2 of the CPL, i.e., the desired DFG-OPC output. As expressed by Eqs. (4) and (5), the effect of the shift in the refractive index between the two DEs in

DFG-OPCs on the output PC wave power is formulated. When $[\{2\beta_2(\omega_s) - \beta_2(\omega_p)\}\{\Delta L + \Delta n(L_2 + \Delta L)\}] = -\pi/2 + 2\pi N$ (N = 0, 1, 2, …), the DFG-OPC output P_{PC2} can be maximized. In the case of $\Delta n = 0$, the maximum DFG-OPC output power can be obtained through the adjustment of the difference in DE lengths, ΔL, appropriately. However, in the case of $\Delta n \neq 0$, the DFG-OPC output P_{PC2} depends not only on ΔL but also on Δn and L_2. The effect of parameters such as Δn and L_2 on the output PC wave power should be studied in detail because it seems difficult to manage the shift Δn in the refractive index with respect to the temperature.

3. Dependence of output PC wave power on shift in refractive indexes between DEs

In this section, the dependence of the output PC wave power on the difference in DE lengths, ΔL, in the presence of the shift Δn in the refractive index and the dependence of the output PC wave power on Δn are examined.

The simulation model is the same as that depicted in Fig. 1. The calculation conditions and parameters are basically identified as done in [14], except for Δn and L_2. For the input waves, the wavelength λ_s and power of the signal wave E_{s2} are 1550 nm and 1 μW, respectively. Thus, the wavelength λ_p and power of the pump wave E_{p2} are 775 nm and 350 mW, respectively. For the DFG-OPC configuration, the splitting ratio of the CPL is 50:50. We assume that a PPLN waveguide is employed as the $\chi^{(2)}$ optical nonlinear material. Its parameters are waveguide length of 5 cm, coupling coefficient κ = 63 $W^{-1/2}m^{-1}$, and polarization inverted period for quasi-phase matching, Λ = 23.9 μm, for $\Delta k = 0$. In addition, the Sellmeier dispersion formula is used to consider dispersion in the PPLN waveguide [28]. The DEs are assumed to be conventional optical fibers. Their phase constant $\beta(\omega)$ is defined as $\beta(\omega) = n(\omega)\omega/c$, where c is the speed of light and the refractive index of the optical fiber $n(\omega)$ is expressed by the experimental formula described in [27]. As described in Section 2, the difference in length between the DEs is $\Delta L = L_1 - L_2$ and the shift in the refractive indexes between the DEs is $\Delta n = n_1/n_2 - 1$.

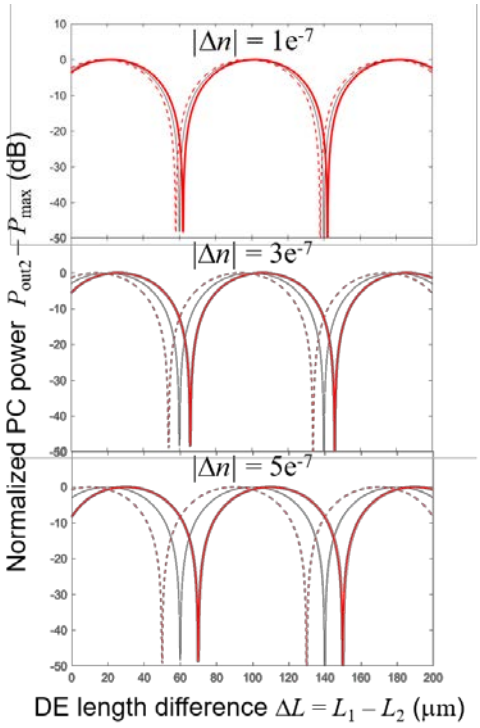

Fig. 2 Normalized output PC wave power $P_{out2} - P_{max}$ as a function of difference in DE lengths, ΔL. Black solid lines indicate $\Delta n = 0$ and dashed and bold solid red lines indicate $+\Delta n$ and $-\Delta n$

Figure 2 depicts the dependence of the output PC wave power on the difference in DE lengths, ΔL, when the shift in the refractive index, $\Delta n \neq 0$. In each graph, the horizontal axis represents the difference in DE lengths, ΔL, and the vertical axis represents the normalized output PC wave power, defined as $P_{PC2} - P_{max}$, where P_{max} is the maximum output PC wave power. The black lines represent the case $\Delta n = 0$. The bold solid red and dashed red lines represent the cases $+\Delta n$ and $-\Delta n$. Figure 2 is calculated for the case L_2 = 20 m, and the top, middle, and bottom figures represent the cases $|\Delta n| = 1e^{-7}$, $3e^{-7}$, and $5e^{-7}$, respectively. When $\Delta n = 0$, the maximum output PC wave power is obtained at ΔL = 20, 100, and 180 μm. However, as $|\Delta n|$ increases, the value of ΔL taking the maximum output PC wave power is changed. Therefore, the output PC power at ΔL = 20, 100, and 180 μm is degraded. For the quantitative evaluation of this phenomenon, the degradation in the output PC wave power, ΔP, is calculated as a function of the shift, Δn, in the refractive index. Figure 3(a) presents the results of the calculation. As depicted in the inset of Fig. 3(a), the degradation ΔP in the output PC wave power is defined as $\Delta P = P_{max} - P_{out2}$ at ΔL_{opt} = 20 μm. The degradation ΔP in the PC optical power increases with the increase in $|\Delta n|$ and displays a convex-function-like trend. Figure 3(b) presents another version of Fig. 3(a), in which the horizontal axis ranges from –10e-6 to +10e-6. Several peaks can be identified for each DE_2 length, L_2 = 5, 10, and 20 m. This is evident from Fig. 2. When $|\Delta n|$ increases, the curve of the output PC wave power shifts. Finally, the value of

this output power reduces to the minimum, although ΔL = 20 μm. Therefore, the degradation ΔP in the PC wave power has local maximum values. It can be seen from Fig. 3(b) that DE_2 with length significantly shorter than 5 m is preferred to avoid degradation in the output PC wave power when the temperature difference between the two DEs is 1.0 °C. This is because there are local maximum values located near Δn = ±8.0e-6 corresponding to the thermo-optical coefficient of 7.814e-6/°C for single-mode fibers [29]. This result indicates that there is a fair chance for the reduction of the degradation in the output PC wave power caused by the shift in the refractive index (temperature fluctuation) by reducing L_2 as much as possible

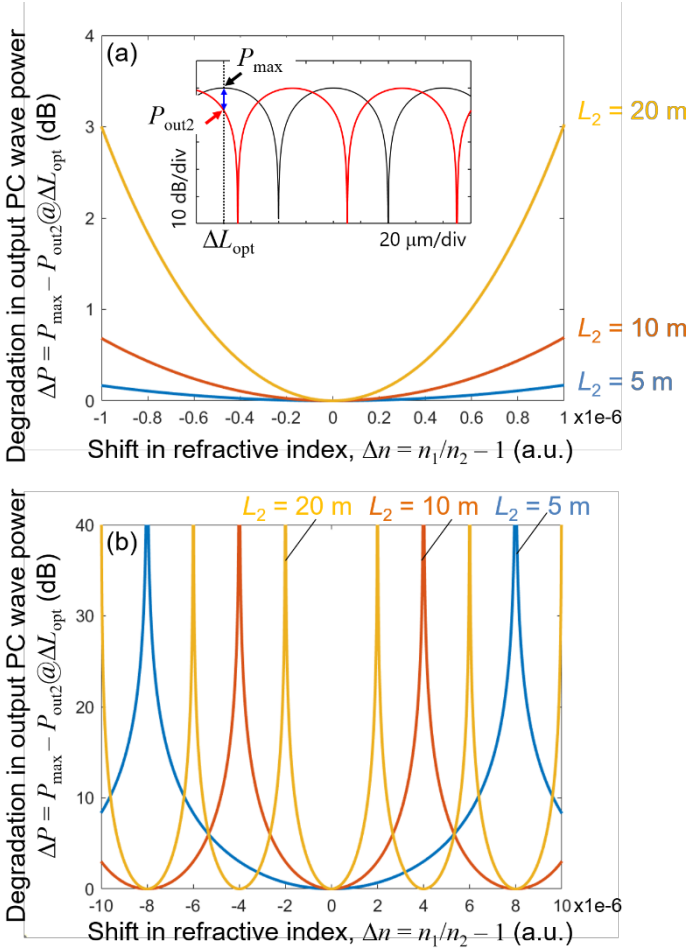

Fig. 3 Degradation ΔP in output PC wave power as function of shift Δn in refractive index. Blue, orange, and yellow lines represent the cases L_2 = 5, 10, 20 m, respectively. (a) Δn ranges from –1.0e-6 to +1.0e-6; (b) Δn ranges from –10.0e-6 to +10.0e-6

4. Dependence of output PC wave power on DE length and acceptable shift in refractive index

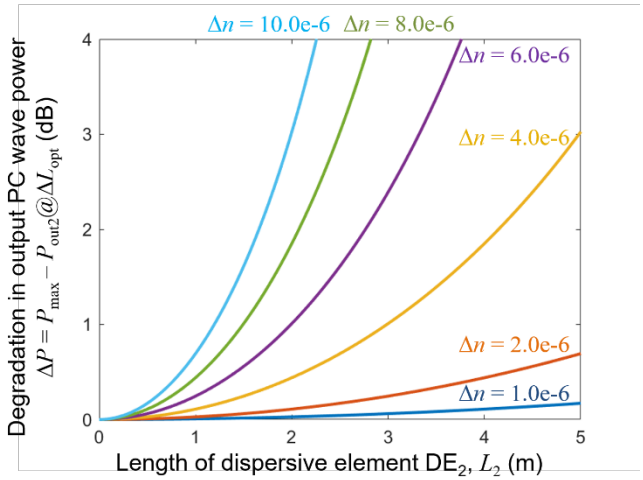

Fig. 4 Degradation ΔP in output PC wave power as function of DE_2 length, L_2. Shift Δn in refractive index varies from 1.0e-6 to 10.0e-6

In this section, the dependence of the output PC wave power on DE_2 length and the acceptable shift in the refractive index is numerically investigated. Figure 4 depicts the degradation ΔP in the output PC wave power as a function of L_2. Each curve indicates the shift Δn, ranging from 1.0e-6 to 10.0e-6. The degradation ΔP in the output PC wave power improves as L_2 reduces. This is because L_2 is the dominant factor of undesired phase shift, which is represented by the term $\Delta n(L_2 + \Delta L)$ in Eq. (5) where ΔL = 20 μm, namely ΔL_{opt}. It is also understood that the optical waves traveling through DEs sense the shift in the refractive index Δn and are phase-shifted in proportion to DE_2 length L_2. As a result, the PC wave partially outputs from port 1 because of the Sagnac loop, and the output PC wave power from port 2 is degraded. Based on this result, the acceptable shift in the refractive index for each L_2 can be determined when the acceptable degradation in the output PC wave power is known, and it would be useful for the design of the DFG-OPC.

Subsequently, the acceptable shift Δn_{tol} in the refractive index is calculated as a function of L_2 and presented in Fig. 5(a). Here, the acceptable degradation in the PC optical power is set to ΔP_{tol}, and the maximum Δn satisfying ΔP_{tol} at a certain value of L_2 is set to Δn_{tol}. In addition, the difference in temperature between the two DEs as a function of L_2 corresponding to Δn_{tol} is depicted in Fig. 5(b). The temperature difference ΔT between the two DEs is defined as $\Delta T = \Delta n_{tol}/(dn/dT)$ [°C]. Assuming that the DEs are single-mode fibers at 20 °C, the thermo-optic coefficient dn/dT is set to 7.814e-6 in these calculations, based on [29].

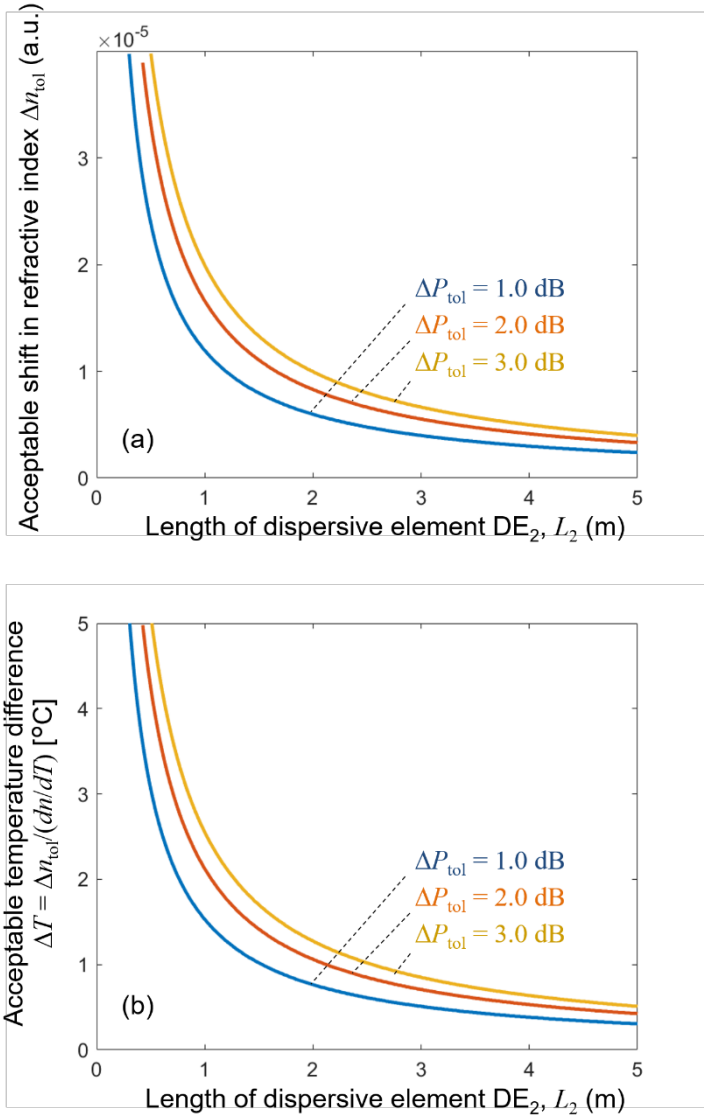

Fig. 5 (a) Acceptable shift in refractive index and (b) temperature difference as a function of DE_2 length, L_2

Figure 5(a) illustrates that Δn_{tol} increases as L_2 reduces. This is because the optical waves traveling through DEs partially sense the shift in the refractive index Δn when L_2 is comparatively shortened, and the undesired phase shift $\Delta n(L_2+\Delta L)$ in Eq. (5) hardly increases by Δn. For example, if the acceptable degradation in the PC optical power is ΔP_{tol} = 1 dB and L_2 = 5 m, Δn_{tol} = 2.4e-6 corresponding to a temperature difference of 0.3 °C, as depicted in Fig. 5(b). This indicates that the temperature settings of DFG-OPCs have to be strictly managed for stable operation. Meanwhile, when L_2 = 1 m, Δn_{tol} = 1.2e-5, which corresponds to a temperature difference of 1.5 °C. In this manner, the requirement of temperature control for the DFG-OPC is relaxed compared with the case when L_2 is longer. From these results, it was numerically clarified that the acceptable shift in the

refractive indexes between the DEs largely depends on L_2. In response to this result, it was also found that it is essential to implement a DE length as short as possible to obtain stable output PC wave power from DFG-OPCs. These results would be useful for the design of DFG-OPCs.

Experimental verification of this study is one of the future works, and Δn control will play an important role in the experiment. The precise temperature control of the DE for the refractive index change must be required and would be a key issue. It also remains a challenge for further research to tune the refractive index dynamically. The thermoelectric cooler(TEC) could enable it. For example, the output power of the PC wave could be stabilized when the temperature of DEs is adaptively controlled with TECs in order that the monitored output PC wave power becomes constant. Additionally, the relatively wide range of the refractive index change could also be achieved by the TEC array along the fiber. For small Δn, the TEC array would be partially used. In contrast, for large Δn, the TEC array would be totally used. It is also expected that the DFG-OPC circuit with Δn control applies to unique applications such as phase-sensitive amplification. In the meantime, novel optical nonlinear media, such as All-optical modulator [30] and Metal-Organic Framework [31] have been studied and have the possibility to show different characteristics from the conventional optical nonlinear medium such as a highly nonlinear optical fiber. The application of such novel optical nonlinear media to OPC will be an interesting topic for future research."

5. Conclusions

In this study, the effect of shift in the refractive indexes between DEs on the output PC wave power of waveband-shift-free DFG-OPCs was analytically investigated. In Section 2, the shift Δn in the refractive index, which has not been considered in earlier studies, was introduced into the DFG-OPC model. The obtained formula showed that not only the difference in DE lengths, ΔL, but also Δn and the DE_2 length, L_2, affect the output PC wave power of DFG-OPCs. In Section 3, the dependence of the output PC wave power on the shift in the refractive index was analytically calculated. The output PC wave power was varied according to Δn. Even for Δn = 1.0e-6, the degradation ΔP in the output PC power was 3 dB when L_2 = 20 m. In Section 4, the dependence of the output PC wave power on L_2 was numerically investigated. The acceptable value of the shift, Δn_{tol}, and the temperature difference ΔT were calculated as functions of L_2. The value of Δn_{tol} increased as L_2 was reduced; therefore, the output PC wave power could be stabilized against changes in temperature. Using the results obtained in this study to design DFG-OPCs, their robustness could be improved.

References

1. Winzer, P. J., Neilson, D. T., Chraplyvy, A. R.,:Fiber-optic transmission and networking: the previous 20 and the next 20 years [Invited]. Opt. Express (2018). https://doi.org/ 10.1364/OE.26.024190
2. Mitra, P. P., Stark, J. B.,:Nonlinear limits to the information capacity of optical fibre communications. Nature (2001). https://doi.org/10.1038/35082518
3. Essiambre, R.-J., Foschini, G. J., Kramer, G., Winzer, P. J.,:Capacity limits of information transport in fiber-optic networks. Phys. Rev. Lett. (2008). https://doi.org/10.1103/PhysRevLett.101.163901
4. Ip, E., Kahn, J. M.,:Compensation of Dispersion and Nonlinear Impairments Using Digital Backpropagation. J. Lightwave Technol. (2008). https://doi.org/10.1109/JLT.2008.927791
5. Ip, E.,:Nonlinear Compensation Using Backpropagation for Polarization-Multiplexed Transmission. J. Lightwave Technol. (2010). https://doi.org/10.1109/JLT.2010.2040135
6. Peddanarappagari, K. V., Brandt-Pearce, M.: Volterra series transfer function of single-mode fibers. J. Lightwave Technol. (1997). https://doi.org/10.1109/50.643545
7. Giacoumidis, E., Le, S. T., Ghanbarisabagh, M., McCarthy, M., Aldaya, I., Mhatli, S., Jarajreh, M. A., Haigh, P. A., Doran, N. J., Ellis, A. D., Eggleton, B. J.: Fiber nonlinearity-induced penalty reduction in CO-OFDM by ANN-based nonlinear equalization. Opt. Lett. (2015). https://doi.org/10.1364/OL.40.005113
8. Hager, C. Pfister, H. D.: Nonlinear interference mitigation via deep neural networks. OFC 2018 (2018). https://doi.org/10.1364/OFC.2018.W3A.4
9. Vasilyev, M.: Distributed phase-sensitive amplification. Opt. Express (2005). https://doi.org/10.1364/OPEX.13.007563
10. Tang, R., Lasri, J., Devgan, P. S., Grigoryan, V., Kumar, P., Vasilyev, M.: Gain characteristics of a frequency nondegenerate phase-sensitive fiber-optic parametric amplifier with phase self-stabilized input. Opt. Express (2005). https://doi.org/10.1364/OPEX.13.010483
11. Tang, R., Devgan, P. S., Grigoryan, V. S., Kumar, P., Vasilyev, M.: In-line phase-sensitive amplification of multi-channel CW signals based on frequency nondegenerate four-wave-mixing in fiber. Opt. Express (2008). https://doi.org/10.1364/OE.16.009046
12. Olsson, S. L. I., Corcoran, B., Lundström, C., Tipsuwannakul, E., Sygletos, S., Ellis, A. D., Tong, Z., Karlsson, M., Andrekson, P. A.: Injection locking-based pump recovery for phase-sensitive amplified links. Opt. Express (2013). https://doi.org/10.1364/OE.21.014512
13. Kazama, T., Umeki, T., Abe, M., Enbutsu, K., Miyamoto, Y., Takenouchi, H.: Low-Parametric-Crosstalk Phase-Sensitive Amplifier for Guard-Band-Less DWDM Signal Using PPLN Waveguides. J. Lightwave Technol. (2017)

https://doi.org/10.1109/JLT.2016.2603186
14. Tian, Y., Huang, Y.-K., Zhang, S., Prucnal, P. R., Wang, T.: Demonstration of digital phase-sensitive boosting to extend signal reach for long-haul WDM systems using optical phase-conjugated copy. Opt. Express (2013). https://doi.org/10.1364/OE.21.005099
15. Yariv, A., Fekete, D., Pepper, D. M.: Compensation for channel dispersion by nonlinear optical phase conjugation. Opt. Lett. (1979). https://doi.org/10.1364/OL.4.000052
16. Schmidt-Langhorst, C., Sackey, I., Elschner, R., Kato, T., Tanimura, T., Watanabe, S., Hoshida, T., Schubert, C.: Fiber Nonlinearity Mitigation in 800-km Transmission of a 1.6-Tb/s Superchannel Using Waveband-Shift-Free Optical Phase Conjugation. ECOC 2017 (2017). https://doi.org/10.1109/ECOC.2017.8346052
17. Sackey, I., Schmidt-Langhorst, C., Elschner, R., Kato, T., Tanimura, T., Watanabe, S., Hoshida, T.: Waveband-Shift-Free Optical Phase Conjugator for Spectrally Efficient Fiber Nonlinearity Mitigation. J. Lightwave Technol. (2018). https://doi.org/10.1109/JLT.2018.2790799
18. Yoshima, S., Sun, Y., Liu, Z., Bottrill, K. R. H., Parmigiani, F., Richardson, D. J., Petropoulos, P.: Mitigation of Nonlinear Effects on WDM QAM Signals Enabled by Optical Phase Conjugation With Efficient Bandwidth Utilization. J. Lightwave Technol. (2017). https://doi.org/ 10.1109/JLT.2016.2623740
19. Saavedra, G., Sun, Y., Bottrill, K. R.H., Galdino, L., Parmigiani, F., Liu, Z., Richardson, D. J., Petropoulos, P., Killey, R. I., Bayvel, P.: Optical phase conjugation in installed optical networks. OFC 2018 (2018). https://doi.org/10.1364/OFC.2018.W3E.2
20. Ellis, A. D., Tan, M., Asif Iqbal, M., Al-Khateeb, M. A. Z., Gordienko, V., Mondaca, G. S., Fabbri, S., Stephens, M. F. C., McCarthy, M. E., Perentos, A., Phillips, I. D., Lavery, D., Liga, G., Maher, R., Harper, P., Doran, N., Turitsyn, S. K., Sygletos, S., Bayvec, P.: 4 Tb/s Transmission Reach Enhancement Using 10 × 400 Gb/s Super-Channels and Polarization Insensitive Dual Band Optical Phase Conjugation. J. Lightwave Technol. (2016). https://doi.org/10.1109/JLT.2016.2521430
21. Umeki, T., Kazama, T., Sano, A., Shibahara, K., Suzuki, K., Abe, M., Takenouchi, H., Miyamoto, Y.: Simultaneous nonlinearity mitigation in 92 × 180-Gbit/s PDM-16QAM transmission over 3840 km using PPLN-based guard-band-less optical phase conjugation. Opt. Express (2016). https://doi.org/10.1364/OE.24.016945
22. Kobayashi, T., Umeki, T., Kasahara, R., Yamazaki, H., Nagatani, M., Wakita, H., Takenouchi, H., Miyamoto, Y.: 96-Gbaud PDM-8QAM single channel transmission over 9,600 km by nonlinear tolerance enhancement using PPLN-based optical phase conjugation. OFC 2018 (2018). https://doi.org/10.1364/OFC.2018.Th3E.4
23. Okamura, Y., Takada, A.: Waveband-shift-free optical phase conjugator based on difference-frequency generation. Opt. Express (2020). https://doi.org/10.1364/OE.387590

24. Mori, K., Morioka, T., Saruwatari, M.: Wavelength-shift-free spectral inversion with an optical parametric loop mirror. Opt. Lett. (1996). https://doi.org/10.1364/OL.21.000110
25. Mori, K., Takara, H., Saruwatari, M.: Wavelength-shift-free FWM based dispersion compensation in non-DSF transmission utilizing optical parametric loop mirror. CLEO 97 (1997). http://doi.org/10.1109/CLEO.1997.603397
26. Okamura, Y., Takada, A.: Influence of Phase Constant Difference between Dispersive Elements in Difference-Frequency Generation Based Optical-Phase-Conjugation Circuit. 24th Microoptics Conference (MOC2019) (2019). https://doi.org/10.23919/MOC46630.2019.8982755
27. Yariv, A., Yeh, P.: Photonics: Optical Electronics in Modern Communications Sixth Edition. Oxford, Oxford (2007)
28. Smith, D. S., Riccius, H. D., Edwin, R. P.: Refractive indices of lithium niobate. Opt. Commun. (1976). https://doi.org/10.1016/0030-4018(76)90273-X
29. Wang, W., Yu, Y., Geng, Y., Li, X.: Measurements of thermo-optic coefficient of standard single mode fiber in large temperature range. 2015 International Conference on Optical Instruments and Technology (2015). https://doi.org/10.1117/12.2193091
30. Lu, L., Wang, W., Wu, L., Jiang, X., Xiang, Y., Li, J., Fan, D., Zhang, H.: All-Optical Switching of Two Continuous Waves in Few Layer Bismuthene Based on Spatial Cross-Phase Modulation. ACS Photonics (2017). http://dx.doi.org/10.1021/acsphotonics.7b00849
31. Jiang, X., Zhang, L., Liu, S., Zhang, Y., He, Z., Li, W., Zhang, F., Shi, Y., Lü, W., Li, Y., Wen, Q., Li, J., Feng, J., Ruan, S., Zeng, Y., Zhu, X., Lu, Y., Zhang, H.: Ultrathin Metal–Organic Framework: An Emerging Broadband Nonlinear Optical Material for Ultrafast Photonics. Adv. Opt. Mater. (2018). https://doi.org/10.1002/adom.201800561